

Tunable Bragg filters with a phase transition material defect layer

Xi Wang,¹ Zilun Gong,^{1,2} Kaichen Dong,^{1,3} Shuai Lou,¹ Jonathan Slack,² Andre Anders,² and Jie Yao^{1,3,*}

¹Department of Materials Science and Engineering, University of California, Berkeley, California 94720, USA

²Accelerator Technology and Applied Physics Division, Lawrence Berkeley National Laboratory, Berkeley, California 94720, USA

³Materials Sciences Division, Lawrence Berkeley National Laboratory, Berkeley, California 94720, USA

**yaojie@berkeley.edu*

Abstract: We propose an all-solid-state tunable Bragg filter with a phase transition material as the defect layer. Bragg filters based on a vanadium dioxide defect layer sandwiched between silicon dioxide/titanium dioxide Bragg gratings are experimentally demonstrated. Temperature dependent reflection spectroscopy shows the dynamic tunability and hysteresis properties of the Bragg filter. Temperature dependent Raman spectroscopy reveals the connection between the tunability and the phase transition of the vanadium dioxide defect layer. This work paves a new avenue in tunable Bragg filter designs and promises more applications by combining phase transition materials and optical cavities.

© 2016 Optical Society of America

OCIS codes: (230.1480) Bragg reflectors; (310.4165) Multilayer design; (160.6840) Thermo-optical materials.

References and links

1. E. Yablonovitch, "Inhibited spontaneous emission in solid-state physics and electronics," *Phys. Rev. Lett.* **58**(20), 2059–2062 (1987).
2. E. Yablonovitch, "Photonic band-gap structures," *J. Opt. Soc. Am. B* **10**(2), 283–295 (1993).
3. S. J. Orfanidis, "Electromagnetic waves and antennas." (2002), <http://www.ece.rutgers.edu/~orfanidi/ewa>.
4. G. Calo, A. D'Orazio, M. De Sario, L. Mescia, V. Petruzzelli, and F. Prudenzano, "Tunability of photonic band gap notch filters," *IEEE Trans. NanoTechnol.* **7**(3), 273–284 (2008).
5. R. Zengerle and O. Leminger, "Phase-shifted Bragg-grating filters with improved transmission characteristics," *J. Lightwave Technol.* **13**(12), 2354–2358 (1995).
6. D. R. Smith, S. L. McCall, P. M. Platzman, R. Dalichaouch, N. Kroll, and S. Schultz, "Photonic band structure and defects in one and two dimensions," *J. Opt. Soc. Am. B* **10**(2), 314–321 (1993).
7. O. Painter, R. K. Lee, A. Scherer, A. Yariv, J. D. O'Brien, P. D. Dapkus, and I. Kim, "Two-dimensional photonic band-Gap defect mode laser," *Science* **284**(5421), 1819–1821 (1999).
8. J. Yoon, W. Lee, J. M. Caruge, M. Bawendi, E. L. Thomas, S. Kooi, and P. N. Prasad, "Defect-mode mirrorless lasing in dye-doped organic/inorganic hybrid one-dimensional photonic crystal," *Appl. Phys. Lett.* **88**(9), 091102 (2006).
9. G. P. Agrawal and S. Radic, "Phase-shifted fiber Bragg gratings and their application for wavelength demultiplexing," *IEEE Photonics Technol. Lett.* **6**(8), 995–997 (1994).
10. T. Erdogan, "Fiber grating spectra," *J. Lightwave Technol.* **15**(8), 1277–1294 (1997).
11. H. C. Kim, K. Ikeda, and Y. Fainman, "Tunable transmission resonant filter and modulator with vertical gratings," *J. Lightwave Technol.* **25**(5), 1147–1151 (2007).
12. Q. Wu and Y. Okabe, "High-sensitivity ultrasonic phase-shifted fiber Bragg grating balanced sensing system," *Opt. Express* **20**(27), 28353–28362 (2012).
13. C. J. S. Matos, P. Torres, L. C. G. Valente, W. Margulis, and R. Stubbe, "Fiber Bragg grating (FBG) characterization and shaping by local pressure," *J. Lightwave Technol.* **19**(8), 1206–1211 (2001).
14. X. Chen, Y. Painchaud, K. Ogusu, and H. Li, "Phase shifts induced by the piezoelectric transducers attached to a linearly chirped fiber Bragg grating," *J. Lightwave Technol.* **28**(14), 2017–2022 (2010).
15. S. Y. Li, N. Q. Ngo, S. C. Tjin, P. Shum, and J. Zhang, "Thermally tunable narrow-bandpass filter based on a linearly chirped fiber Bragg grating," *Opt. Lett.* **29**(1), 29–31 (2004).
16. Q. Zhu and Y. Zhang, "Defect modes and wavelength tuning of one-dimensional photonic crystal with lithium niobate," *Optik (Stuttg.)* **120**(4), 195–198 (2009).
17. C. J. Wu, J. J. Liao, and T. W. Chang, "Tunable multilayer Fabry-Perot resonator using electro-optical defect layer," *J. Electromagnet. Wave.* **24**(4), 531–542 (2010).

18. P. Halevi and F. Ramos-Mendieta, "Tunable photonic crystals with semiconducting constituents," *Phys. Rev. Lett.* **85**(9), 1875–1878 (2000).
19. H. C. Hung, C. J. Wu, and S. J. Chang, "A mid-infrared tunable filter in a semiconductor-dielectric photonic crystal containing doped semiconductor defect," *Solid State Commun.* **151**(22), 1677–1680 (2011).
20. J. López, L. E. González, M. F. Quiñonez, N. Porras-Montenegro, G. Zambrano, and M. E. Gómez, "Band structure of a 2d photonic crystal based on ferrofluids of $\text{Co}_{0.8}\text{Zn}_{0.2}\text{Fe}_2\text{O}_4$ nanoparticles under perpendicular applied magnetic fields," *J. Phys. Conf. Ser.* **480**(1), 012033 (2014).
21. Y. K. Ha, Y. C. Yang, J. E. Kim, H. Y. Park, C. S. Kee, H. Lim, and J. C. Lee, "Tunable omnidirectional reflection bands and defect modes of a one-dimensional photonic band gap structure with liquid crystals," *Appl. Phys. Lett.* **79**(1), 15–17 (2001).
22. R. Ozaki, T. Matsui, M. Ozaki, and K. Yoshino, "Optical property of electro-tunable defect mode in 1d periodic structure with light crystal defect layer," *Electron. Commun.* **2** **87**(5), 24–31 (2004).
23. R. Ozaki, M. Ozaki, and K. Yoshino, "Defect mode in one-dimensional photonic crystal with in-plane switchable nematic liquid crystal defect layer," *Jpn. J. Appl. Phys.* **43**, 1477–1479 (2004).
24. F. J. Morin, "Oxides which show a metal-to-insulator transition at the Neel temperature," *Phys. Rev. Lett.* **3**(1), 34–36 (1959).
25. H. W. Verleur, A. S. Barker, and C. N. Berglund, "Optical properties of VO_2 between 0.25 and 5 eV," *Phys. Rev.* **172**(3), 788–798 (1968).
26. M. Imada, A. Fujimori, and Y. Tokura, "Metal-insulator transitions," *Rev. Mod. Phys.* **70**(4), 1039–1263 (1998).
27. J. Wu, Q. Gu, B. S. Guiton, N. P. de Leon, L. Ouyang, and H. Park, "Strain-induced self organization of metal-insulator domains in single-crystalline VO_2 nanobeams," *Nano Lett.* **6**(10), 2313–2317 (2006).
28. A. Perucchi, L. Baldassarre, P. Postorino, and S. Lupi, "Optical properties across the insulator to metal transitions in vanadium oxide compounds," *J. Phys. Condens. Matter* **21**(32), 323202 (2009).
29. J. Cao, E. Ertekin, V. Srinivasan, W. Fan, S. Huang, H. Zheng, J. W. L. Yim, D. R. Khanal, D. F. Ogletree, J. C. Grossman, and J. Wu, "Strain engineering and one-dimensional organization of metal-insulator domains in single-crystal vanadium dioxide beams," *Nat. Nanotechnol.* **4**(11), 732–737 (2009).
30. H.-T. Kim, B.-J. Kim, S. Choi, B.-G. Chae, Y. W. Lee, T. Driscoll, M. M. Qazilbash, and D. N. Basov, "Electrical oscillations induced by the metal-insulator transition in VO_2 ," *J. Appl. Phys.* **107**(2), 023702 (2010).
31. A. Cavalleri, T. Dekorsy, H. H. W. Chong, J. C. Kieffer, and R. W. Schoenlein, "Evidence for a structurally-driven insulator-to-metal transition in VO_2 : A view from the ultrafast timescale," *Phys. Rev. B* **70**(16), 161102 (2004).
32. J. B. Kana Kana, J. M. Ndjaka, G. Vignaud, A. Gibaud, and M. Maaza, "Thermally tunable optical constants of vanadium dioxide thin films measured by spectroscopic ellipsometry," *Opt. Commun.* **284**(3), 807–812 (2011).
33. G. I. Petrov, V. V. Yakovlev, and J. Squier, "Raman microscopy analysis of phase transformation mechanisms in vanadium dioxide," *Appl. Phys. Lett.* **81**(6), 1023–1025 (2002).
34. C. Cheng, K. Liu, B. Xiang, J. Suh, and J. Wu, "Ultra-long, free-standing, single-crystalline vanadium dioxide micro/nanowires grown by simple thermal evaporation," *Appl. Phys. Lett.* **100**(10), 103111 (2012).
35. T. Driscoll, H.-T. Kim, B.-G. Chae, B.-J. Kim, Y.-W. Lee, N. M. Jokerst, S. Palit, D. R. Smith, M. Di Ventra, and D. N. Basov, "Memory metamaterials," *Science* **325**(5947), 1518–1521 (2009).
36. M. J. Dicken, K. Aydin, I. M. Pryce, L. A. Sweatlock, E. M. Boyd, S. Walavalkar, J. Ma, and H. A. Atwater, "Frequency tunable near-infrared metamaterials based on VO_2 phase transition," *Opt. Express* **17**(20), 18330–18339 (2009).
37. M. D. Goldflam, T. Driscoll, B. Chapler, O. Khatib, N. Marie Jokerst, S. Palit, D. R. Smith, B.-J. Kim, G. Seo, H.-T. Kim, M. D. Ventra, and D. N. Basov, "Reconfigurable gradient index using VO_2 memory metamaterials," *Appl. Phys. Lett.* **99**(4), 044103 (2011).
38. A. Cavalleri, C. Tóth, C. W. Siders, J. A. Squier, F. Ráksi, P. Forget, and J. C. Kieffer, "Femtosecond structural dynamics in VO_2 during an ultrafast solid-solid phase transition," *Phys. Rev. Lett.* **87**(23), 237401 (2001).
39. A. Crunteanu, J. Givernaud, J. Leroy, D. Mardivirin, C. Champeaux, J.-C. Orliaanges, A. Catherinot, and P. Blondy, "Voltage- and current-activated metal-insulator transition in VO_2 -based electrical switches: a lifetime operation analysis," *Sci. Technol. Adv. Mater.* **11**(6), 065002 (2010).
40. Y. Zhou, X. Chen, C. Ko, Z. Yang, C. Mouli, and S. Ramanathan, "Voltage-triggered ultrafast phase transition in vanadium dioxide switches," *IEEE Electron Device Lett.* **34**(2), 220–222 (2013).
41. S. Lysenko, A. Rúa, V. Vkhnin, F. Fernández, and H. Liu, "Insulator-to-metal phase transition and recovery processes in VO_2 thin films after femtosecond laser excitation," *Phys. Rev. B* **76**(3), 035104 (2007).

1. Introduction

Bragg gratings, as famous one-dimensional photonic crystals, are formed by alternating dielectric layers with different refractive indices [1, 2]. Featured with designable highly reflected wavelengths (photonic bandgap), this mature technic has led to plenty of applications, including dielectric mirrors and optical filters [3, 4]. With the introduction of a defect layer to break the symmetry, phase-shifted Bragg gratings exhibit unique behaviors as ultra-narrow band-pass filters [5], namely Bragg filters. A Bragg filter works in either reflection mode or transmission mode. While the majority of light near the Bragg wavelength

is reflected, a narrow band (known as a defect mode) gives rise to a reflection dip or transmission peak [3, 6]. Bragg filters with tunable defect modes attract much attention due to their potential abilities for laser cavities [7, 8], sensing, communications, and spectroscopy applications [9–12]. By changing the property of a defect layer, such as its refractive index or thickness, the reflection dip (transmission peak) can be tuned accordingly. However, once the structure of a Bragg filter is determined during the fabrication process, the defect mode is spectrally fixed in most designs. To date, tunability of Bragg filters is primarily based on mechanical stretching [13, 14], or using a thermal-optic effect [15] in optical fibers, which calls for about 20-mm-long fiber and cannot be applied to free space optics directly. Though new tuning mechanisms for planar Bragg filters have been theoretically proposed using piezoelectric materials [16, 17], doped semiconductors [18, 19], and magnetic materials [20] as defect layers, only liquid-crystal-based tunable Bragg filters have been realized in laboratories [21–23]. Moreover, devices containing liquid crystal layer(s) require additional fabrication processes for confinement and stabilization.

Here, we experimentally demonstrate an all-solid-state tunable Bragg filter with a phase transition material as the defect layer. Phase transition materials, especially insulator-metal transition (IMT) materials, exhibit huge changes in electrical, mechanical and optical properties as a function of temperature and/or strain [24–30], which could give optical devices extra tunability.

Without loss of generality, we use vanadium dioxide (VO_2) as the phase transition material for a defect layer because its phase transition temperature ($\sim 68^\circ\text{C}$) is close to room temperature. The IMT of VO_2 occurs between a dielectric monoclinic phase at lower temperatures and a metallic rutile phase at higher temperatures [31]. The temperature dependent optical constants of VO_2 have been reported previously using ellipsometry [32]. Though known as metallic phase at high temperature, in the wavelength region between 500 nm and 1000 nm, the optical properties of VO_2 stay as dielectric (real part of relative permittivity > 0) under both phases, but with dramatic difference. Considering dispersion in the wavelength region from 500 to 1000 nm, the complex refractive index of VO_2 varies from $3.6 + 0.6i$ to $3.0 + 0.5i$ at room temperature, and from $3 + 0.8i$ to $1.5 + 1.4i$ at high temperature (around 80°C). This confirms VO_2 to be a good candidate of a tunable defect layer. In addition, the intrinsic phase transition properties of VO_2 are preserved after the VO_2 layer is encapsulated between two Bragg gratings. This promises more potential applications by combining phase transition materials with optical cavities.

2. Experiment

2.1 Fabrication

Bragg filters fabricated in our experiment consist of one VO_2 thin film (30 nm) with one silicon nitride (Si_3N_4) protection layer (9 nm) sandwiched between two Bragg gratings with 4 periods of alternating titanium dioxide (TiO_2) and silicon dioxide (SiO_2) layers. The schematic diagram with cross-section view can be found in Fig. 1. The whole sample was produced on a quartz substrate in a customized magnetron sputtering system. All the layers were deposited in one chamber continuously without breaking the vacuum, minimizing contamination.

The chamber was pumped down to 6×10^{-7} Torr before any film growth. The TiO_2 and VO_2 film deposition was carried out by DC reactive sputtering from a titanium target (99.995%, ACI Alloys) and a vanadium target (99.9%, ACI Alloys) respectively. The SiO_2 and Si_3N_4 film were produced by RF reactive sputtering from an undoped silicon target (99.999%, ACI Alloys). During the deposition of TiO_2 , SiO_2 and VO_2 , a mixture of argon (Ar) and oxygen (O₂) was introduced into the chamber as working gas, while only pure nitrogen (N₂) was involved during the Si_3N_4 deposition. The $\text{TiO}_2/\text{SiO}_2$ multi-layer forms the Bragg filter structure, and the VO_2 and Si_3N_4 films act as the defect layer in the Bragg filter.

A 9 nm Si_3N_4 layer was deposited on top of VO_2 film to protect VO_2 from subsequent oxygen plasma back-sputtering.

All the films besides the VO_2 film were deposited at room temperature, but a heating effect was anticipated due to plasma bombardment. The sample tray receiver (copper) was heated by 4 cartridge heaters (McMaster-Carr) prior to VO_2 film deposition to achieve a high quality polycrystalline VO_2 film. The heat is transferred by radiation and conduction to the quartz substrate, the temperature of which is raised to around 350 °C. A photo of a typical Bragg filter sample is shown in the inset of Fig. 1. Layers' thicknesses of three fabricated Bragg filter samples are summarized in Table 1.

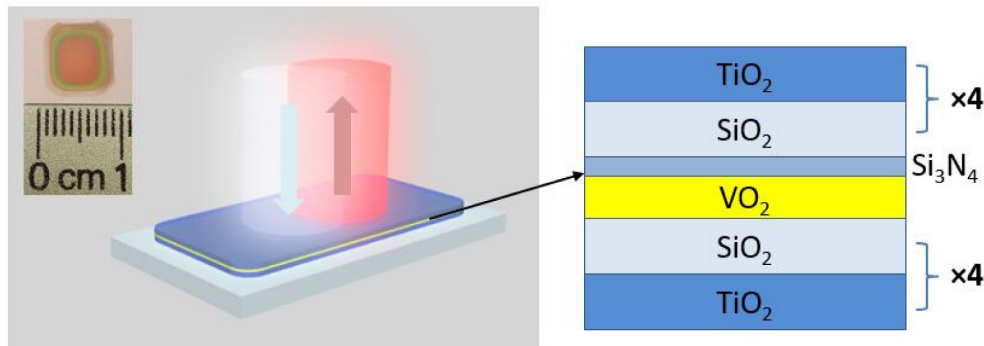


Fig. 1. Schematic diagram with cross-section view and photo (inset) of a typical tunable Bragg filter sample. The figure is not drawn to the scale.

Table 1. Layers' thicknesses of different Bragg filter samples

Sample	SiO_2 (nm)	TiO_2 (nm)	VO_2 (nm)	Si_3N_4 (nm)
A	86	110	30	9
B	77	94	30	9
C	80	102	30	9

2.2 Characterization

Spectral responses of the fabricated Bragg filter samples were characterized. Samples were mounted on a thermal stage with temperature controller, which was set to a slow ramp rate of 2 K/min to minimize possible hysteresis from over heating or cooling. White light from a quartz tungsten source (LSH-100, Horiba) was reflected by a sapphire beam splitter and focused on the surface of samples by a $40 \times$ objective lens. A cutting edge aperture was placed at the image plane behind the beam splitter to select a sample area ($\sim 50 \mu\text{m}$ diameter) from the reflected light. Then the selected light is focused into a spectrometer (iHR320, Horiba) and normalized to the reflection spectrum of a silver mirror. Also, temperature dependent Raman spectroscopy was performed directly on the Bragg filter samples as well as a single VO_2 layer. While using a commercial Raman system (Renishaw Invia instrument with an excitation laser wavelength of 488 nm and a $50 \times$ objective lens) to record the Raman spectra during the heating and cooling processes, identical temperature control as in the optical measurements was used. The excitation wavelength is chosen outside the bandgap of the Bragg gratings. The focused laser spot was $\sim 3 \mu\text{m}$ in diameter and Raman spectra were taken with low laser power ($\sim 20 \mu\text{W}$) to minimize undesired over-heating effect.

3. Results and discussion

Raman spectroscopy has been used to verify the composition of the defect film. The Raman spectrum of the Bragg filter sample A at 25 °C is shown in Fig. 2(a) with the Raman spectrum of a single VO_2 layer on SiO_2/Si substrate as a reference. It is clear that though with lower contrast, typical Raman peaks of VO_2 (including A_g and B_g modes at 196 cm^{-1} , 225 cm^{-1} , 261

cm^{-1} , 309 cm^{-1} , 390 cm^{-1} , and 612 cm^{-1}) in the Bragg filter match well with the Raman peaks of single VO_2 layer [33, 34]. This means even being encapsulated between two multilayer gratings, the defect layer is still an active polycrystalline VO_2 . Possible influence from strain on the material properties is small or negligible.

Our Bragg filter samples exhibit temperature-dependent tunability. The reflection spectra of sample A under different temperature are shown on Figs. 2(b) and 2(c). At shorter wavelength region, the reflectance is almost invariant at all temperatures. At longer wavelength region, the reflectance, especially the position of defect mode, changes dramatically. The center wavelength of the defect mode (dip of reflectance) changes from 795 nm to 742 nm when the temperature increases from 25°C to 83°C , shown in Fig. 2(b), and goes back from 742 nm to 795 nm during the cooling process shown in Fig. 2(c). To further confirm the ubiquity of such tunability, the reflection spectra of Bragg filter samples B and C with different grating thicknesses are shown in Figs. 2(d) and 2(e). The temperature-dependent shifts of defect modes are evident.

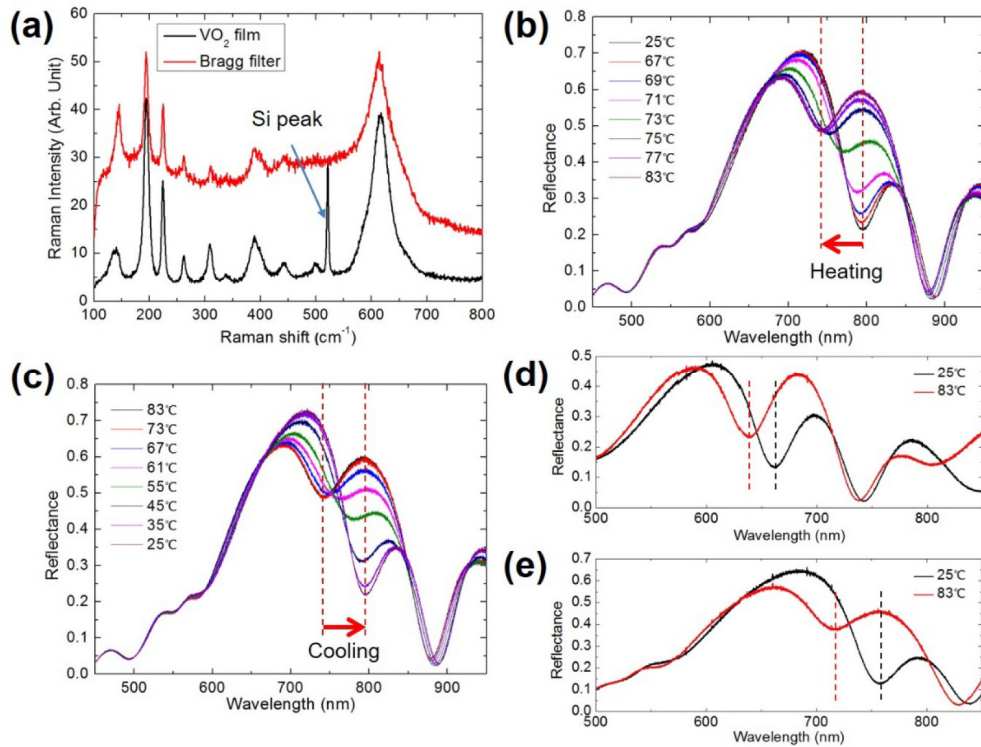


Fig. 2. (a) The Raman spectrum of the Bragg filter sample A at 25°C (red) and the Raman spectrum of a single layer VO_2 on SiO_2/Si substrate (black). The Raman peak of silicon substrate is indicated by an arrow; the reflection spectra of sample A during (b) heating and (c) cooling processes. Red arrows indicate shifts of reflection dips during heating and cooling respectively. The reflection spectra under 25°C and 83°C for Bragg filter samples (d) B and (e) C. Dots lines indicate the reflection dips of defect modes.

One prominent phenomenon in the IMT phase transition of VO_2 is the hysteresis behavior, which was first observed in electric conductivity [24], then confirmed optically [25]. This unique property has been utilized in many optical applications [35–37]. In our experiment, optical hysteresis was also observed. Considering the sample A and plotting the center wavelengths of defect mode versus temperatures during the whole heating and cooling cycle, a hysteresis curve is obtained (Fig. 3(a)). During the heating and cooling processes, the windows of significant changing are at $\sim 10^\circ\text{C}$ and $\sim 40^\circ\text{C}$, respectively. Therefore, the

tuning of defect modes can be realized in a much narrower temperature range than those using thermal-optic effects [18]. More importantly, this hysteresis in reflection tuning has the potential to bring about memory-like function [35], thus further enriches the potential applications of Bragg filter devices.

Temperature dependent Raman spectroscopy verifies that the tunability of our Bragg filter originates from the phase transition of the VO_2 layer. According to literature [33], the Raman shift at 612 cm^{-1} is able to characterize the hysteresis of the VO_2 MIT phase transition. Heights of 612 cm^{-1} Raman shift of the Bragg filter sample are retrieved from Raman spectra under different temperatures and plotted in red in Fig. 3(b). The hysteresis shape of this curve is almost identical to that of the defect mode shift shown in Fig. 3(a). More compelling evidence of the origin of hysteresis is given by plotting the reversed reflectance ($-1 \times$ reflectance) at 795 nm during the whole heating and cooling cycle (blue curve in Fig. 3(b)). This reflection hysteresis curve perfectly matches the hysteresis curve of Raman spectra. As a conclusion, the characterization results show that the Bragg filter is tuned by the phase transition of the VO_2 defect layer.

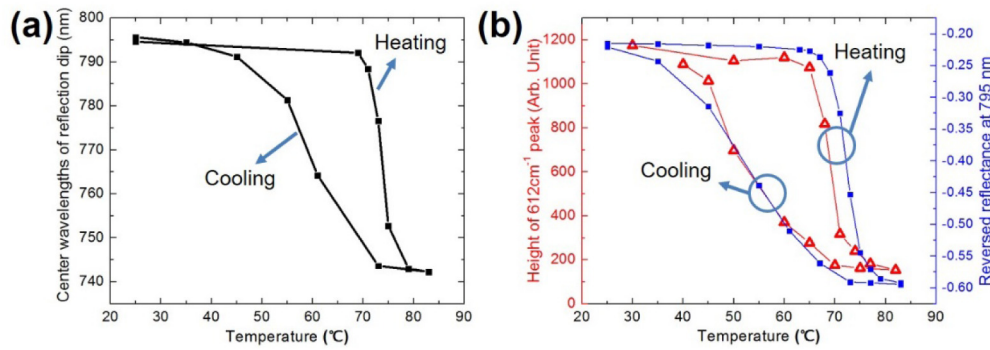


Fig. 3. (a) A hysteresis curve of the center wavelengths of defect modes (reflection dips); (b) Heights of 612 cm^{-1} Raman shift of the Bragg filter sample retrieved from Raman spectra (red) and reversed reflectance at 795 nm (blue) as a function of temperature.

The design process is relatively straight forwards: we design Bragg grating layers using $\lambda_B = 2(n_1d_1 + n_2d_2)$, (n_i and d_i are the refractive index and thickness of corresponding alternating layers) to meet our specific working wavelength region; then a VO_2 defect layer is inserted into the center of the Bragg grating to produce defect modes. Accurate relations between the thickness of the VO_2 layer and defect modes are studied by numerical simulations.

We have done numerical simulations using COMSOL Multiphysics® and compared with our experimental results. In the simulation setup, the refractive indexes of SiO_2 , TiO_2 and Si_3N_4 are set to 1.46, 2.4 and 2 respectively. The dispersive complex optical refractive index of VO_2 is adopted from Ref [32]. The small variation in temperatures (25 °C vs 30 °C, 83 °C vs 85 °C) doesn't provide notable amount of results difference because optical parameters of VO_2 change very slowly in either low temperature or high temperature region. Fig. 4(a) shows the simulation results of the sample A together with the experimental results. Dashed lines indicate positions of corresponding defect modes. We find that the positions and bandwidths of defect modes agree well with the simulated values. The small shift of Bragg wavelength may result from dispersive optical parameters in real materials. The overall lower reflectance comes from the scattering of polycrystalline TiO_2 , which annealed during high temperature VO_2 layer deposition. This drawback can be solved by alternative materials with higher temperature tolerance to fabricate Bragg gratings.

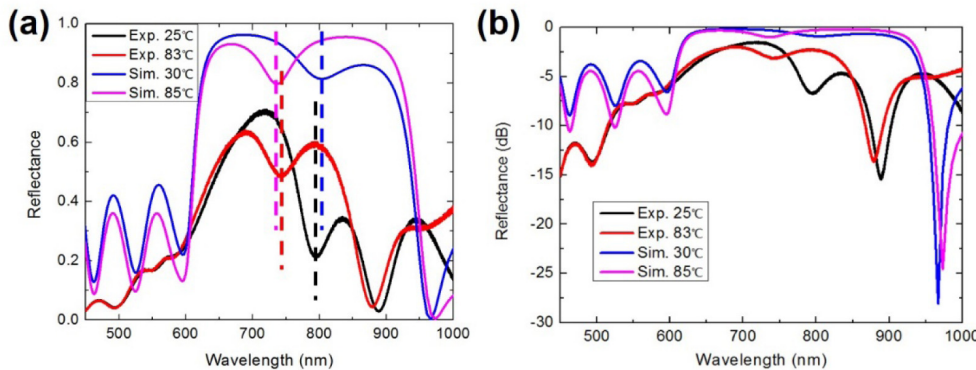


Fig. 4. (a) Simulated and experimental reflection spectra of sample A. Dashed lines indicate positions of corresponding defect modes. (b) Simulated and experimental reflection spectra of sample A plotted in dB showing insertion losses.

It is worth mentioning that, though the full width at half maximum (FWHM) of defect modes in our Bragg filters are wider than those in typical Bragg filters, the defect mode shifts we demonstrated (~ 50 nm) are still larger than the FWHM (~ 40 nm). To make better use of such Bragg filter, small FWHM of defect modes is preferred. The broadening of defect modes results from the optical loss of VO_2 . If a phase transition material with lower loss is encapsulated as a defect layer of Bragg filters, the FWHM of defect modes is expected to be much narrower.

We have also investigated the insertion loss by plotting the reflection spectrum in dB as shown in Fig. 4(b). In the long wavelength region, the insertion losses are about -4 dB in experiments. In the short wavelength region, due to the scattering from polycrystalline TiO_2 , the experimental insertion losses are about 5 dB higher.

Since Bragg filters are tuned by the phase of VO_2 , the modulation speed is determined by the phase transition speed of VO_2 . The global heating method used in our experiment is just for demonstration purposes. There are multiple faster and more energy efficient methods to improve the performance of Bragg filters. It has been reported that the switching time can be very short. For application purposes, we need to include a full cycle of insulator-metal-insulator, not only the intrinsic ultrafast insulator-to-metal transition which happens in a few ps [38]. Very short switching times have been reported: 5 μs by electrical heating [39], 3 μs by applying an electric field [40] and 200 ns by an optical pump-probe method [41].

4. Conclusions and outlook

In conclusion, we have experimentally demonstrated a tunable Bragg filter using a phase transition material, i.e. VO_2 , as the defect layer. Temperature-dependent Raman spectroscopy verified that this device is tuned by the phase transition of VO_2 . This work promises more applications by combining phase transition materials and optical cavities in different ways.

First, our device is the first compact planar all-solid-state tunable Bragg filter, and greatly enriches the application scenarios of Bragg filters. Such designs are not only feasible for practical environments, but also promising for on-chip optical devices and electro-optical modulation.

Second, the combination of phase transition materials and Bragg reflectors could directly transfer the history of environment to optical signals, thus enables remote sensing and control. The device we demonstrate shows the potential of a memory-like passive temperature sensor, or electrical sensor if we integrate current heating.

Third, the sandwich structure also solves the problem of material degradation. Many phase transition materials, including VO_2 , are sensitive to oxygen and/or moisture because of

multivalence of transition metal elements. However, the Bragg reflectors on both sides of the defect layers make the device robust and more practical in applications.

In all, we are looking forward to seeing more exciting devices based on tunable Bragg filters and their commercialization.

Funding

Samsung Advanced Institute of Technology (037361-003); the Laboratory Directed Research and Development Program of Lawrence Berkeley National Laboratory under U.S. Department of Energy Contract (DE-AC02-05CH11231).

Acknowledgments

We thank the generous support from Prof. Junqiao Wu.